Citation for published version:
Hamaza, S, Georgilas, I & Richardson, TS 2018, An Adaptive-Compliance Manipulator for Contact-Based Aerial Applications. in IEEE International Conference on Advanced Intelligent Mechatronics. IEEE.

Publication date:
2018

Document Version
Peer reviewed version

Link to publication

University of Bath

An Adaptive-Compliance Manipulator for Contact-Based Aerial Applications

Salua Hamaza[1], Ioannis Georgilas[2], Thomas Richardson[1,3]

Abstract— This paper presents simulation and airborne test results for a quadrotor equipped with an actively-variable compliance manipulator for contact interaction. Typical applications of this type of manipulator might include sensor placement operations and non-destructive testing. It is shown that through the use of the proposed manipulator, the force experienced at the end-effector can be adaptively controlled, and the effect of interactions on the aircraft itself minimised. Simulation and airborne results show a consistent correlation between the peak loads experienced at the end-effector and the actuator gains. A lightweight, adaptively-compliant actuator of this type offers the opportunity not only to tailor different demanded forces at the end-effector, but also to shape the loads applied - effects which can be achieved by changing only the software structure and tuning of the actuator control system.

I. INTRODUCTION

Unmanned Aerial Vehicles (UAVs) are agile aerial systems, used with a variety of sensors that allow autonomous operation in different scenarios. So far, visual sensing has been used widely for several missions such as police and civil security; fire and rescue; distribution network monitoring in the energy sector and environmental surveying. Since 2009 manipulation capabilities have been encompassed within the aerial platform [1] and this gave scope for a new research area, *aerial manipulation*.

Aerial manipulation has its dawn in slung load transportation and deployment by a single [2]–[4] or multiple UAVs [5]–[7]. More recent work focuses on the interaction with the environment for performing tasks such as non-destructive testing [8] or simple maintenance operations conducted in quasi-static conditions [9]–[11].

This work addresses the challenges of aerial dynamic interaction and proposes a novel lightweight actuator that features adaptive compliance. This is a key feature for a manipulator that interacts with unknown objects; in particular the adaptive behaviour ensures higher flexibility as opposed to the use of constant-stiffness springs, and alleviates undesired disturbances experienced by the aircraft. Adaptive compliance is achieved through the use of a closed-loop controller on the actuator which allows to define both the demanded force at the end-effector and the demanded speed of application of such force, i.e. a high force in a short period of time as opposed to a slow force over a longer period.

[1] Bristol Robotics Laboratory, University of Bristol and University of the West of England, Bristol, UK. *s.hamaza@bristol.ac.uk

[2] Dept. of Mechanical Engineering, University of Bath, Bath, UK.

[3] Dept. of Aerospace Engineering, University of Bristol, Bristol, UK.
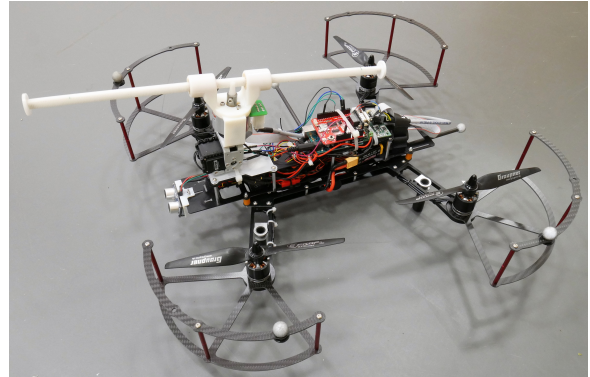
Fig. 1: A quadcopter equipped with an adaptive-compliance manipulator for contact-based interaction.

The application envisioned is the positioning of small objects, e.g. sensors, onto large-scale infrastructure, e.g. dams, bridges, wind turbines. For this type of task, the aircraft is likely to be operating in open space where gusts and other external disturbances can occur. Hence the use of an adaptive-compliance manipulator becomes necessary during the placement task in order to mitigate the propagation of such disturbances to the aircraft. In fact, this type of manipulator can be seen as a mechanical filter as it absorbs/exerts forces independently of the motion of the vehicle, bringing a benefit to the UAV stability. Lastly, the adaptive-compliance manipulator also ensures a secure interface between the sensor and the target object, and it is essential when interacting with delicate surfaces in order to apply a controlled force at all times.

Background

Aerial physical interaction has been an area of keen interest in the past 5 years. The state-of-the-art shows that *aerial manipulators* have been able to exert forces of up to 5N [9], [12] with several design approaches.

The benefits of adding compliance, either in hardware or software, as a feature of the aerial manipulator has been demonstrated in several works. Compliance achieved mechanically is validated in [13], [14] where a passively compliant manipulator comprising a spring-lock mechanism is used for impact absorption and stable contact with a vertical wall. The reaction forces experienced by the end-effector during an impact drastically decrease as the passive element is deployed. In [15] a bio-inspired lightweight arm features active compliance which allows for payload estimation thanks to the elongation of a linear element. The payload estimate is then fed into the flight controller to compensate for any loss in altitude while grasping an object. In [16]

a compliant finger module is added to detect soft collision and obstacle localization by measuring the deflection of the compliant element. In [17] it is presented a collision-resilient flying robot encapsulated within a protection case which enables impact absorption thanks to the material properties of the compliant surrounding structure. Similarly, in [18] a passive gimbal mounted on a protective frame transforms the linear kinetic energy of an impact into rotational while preserving the position of the UAV's centre of gravity (CoG), hence minimising the propagation of disturbances.

As for compliance implemented in software, works in [19]–[21] demonstrate that compliant control aids force estimation and motion feedback at the end-effector, improving stable contact during interaction. Other research questions consider the negative effect of moving masses on both the attitude and altitude dynamics. Hence, changes to the UAV's CoG should be minimised to improve flight stability and battery endurance [22].

Building on the work that has been identified above, we propose a novel lightweight actuator design that features actively-variable compliance to achieve safe and stable interaction, and the ability to absorb undesired forces independently of the vehicle motion.

II. AERIAL MANIPULATOR DYNAMICS

In this section, a brief description of the mathematical model for a multi-rotor vehicle carrying an external load is presented. The dynamics of aerial manipulators are already examined in the literature [5]–[7], [10], [23], the basis of which we use here to identify the key parameters that drive the design decisions for a bespoke manipulator.

Aerial Vehicle Model

Let us consider a generic aerial platform with n-rotors modeled as a rigid body that moves with 6 DoFs in space. We define two coordinate frames as illustrated in fig. 2, one is the ground-fixed frame $\mathcal{W}$ and the other is the aircraft-fixed frame $\mathcal{A}$ which moves relatively to $\mathcal{W}$ and its origin we assume to coincide with the aircraft centre of gravity (CoG). The pose of the vehicle is described relative to the ground-fixed frame as a column vector $\mathbf{p}$ with translation and rotational terms: $\mathbf{p} = [\zeta_x \; \zeta_y \; \zeta_z \; \phi_R \; \theta_P \; \psi_Y]^T$. The equation of
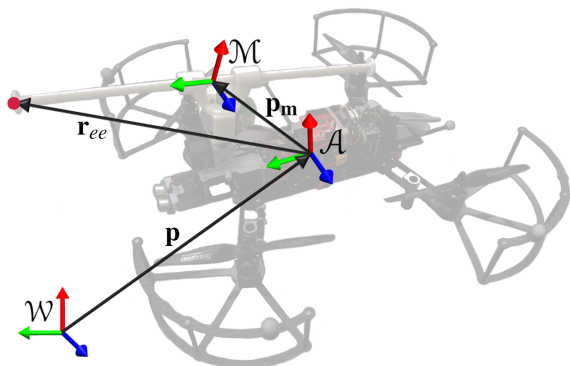

Fig. 2: Aerial manipulator sketch and coordinate frames.

motion of the system is:

$$\mathbf{M}\ddot{\mathbf{p}} + \mathbf{C}(\mathbf{p},\dot{\mathbf{p}})\dot{\mathbf{p}} + \mathbf{G}(\mathbf{p}) = \tau + \tau_{\mathbf{man}} \quad (1)$$

where $\mathbf{M}$ is the mass matrix representing the inertial terms of the system, $\mathbf{C}$ is a skew-symmetric matrix representing the centripetal and Coriolis terms of the damped system, $\mathbf{G}$ is the gravitational term representing forces acting on the system due to gravity. The right side of the equation has τ representing the control torques and forces generated by the n-rotors of the aircraft, i.e. the n-torques and the overall thrust force. Finally $\tau_{\mathbf{man}} = [\mathbf{F_m} \; \mathbf{M_m}]^T$ represents the vector of the external forces and moments generated by the presence of the manipulator.

Manipulator Model

For the calculation of $\mathbf{F_m}$ and $\mathbf{M_m}$ and their effect we will start by representing the manipulator as an external mass suspended on the aircraft. We define a coordinate frame $\mathcal{M}$ centred in the manipulator's CoG. As the manipulator is deployed to perform a task, the position of its CoG will vary independently from the aircraft. Hence, the pose of the manipulator's CoG with respect to frame $\mathcal{A}$ is expressed by vector $\mathbf{p_m} = [\zeta_{mx} \; \zeta_{my} \; \zeta_{mz} \; \phi_{mR} \; \theta_{mP} \; \psi_{mY}]^T$. The manipulator's equation of motion is:

$$\mathbf{M}\ddot{\mathbf{p}}_\mathbf{m} + \mathbf{C}(\mathbf{p_m},\dot{\mathbf{p}}_\mathbf{m})\dot{\mathbf{p}}_\mathbf{m} + \mathbf{G}(\mathbf{p_m}) = \sigma_{\mathbf{ext}} \quad (2)$$

where $\mathbf{M}$ is the mass matrix of the system, $\mathbf{C}$ is the damping matrix containing centripetal and Coriolis terms and $\mathbf{G}$ is the matrix describing the gravitational terms. For the equilibrium, the left side equates the sum of all external forces and moments σ_{ext} acting on the manipulator, for example due to interaction. It is to be noted that eq. (2) does not consider the dynamic effects of the aerial vehicle (see eq. (1)) as this model is solely describing the manipulator dynamics.

Now, let us define vector $\mathbf{r}_{ee} = [x_{ee} \; y_{ee} \; z_{ee}]^T$ as the vector connecting the origin of frame $\mathcal{A}$ to the tip of the end-effector, as shown in fig. 2. The external forces and moments acting on the aircraft due to the interaction between the end-effector and the environment, expressed in frame $\mathcal{A}$ are:

$$\sigma_{ext} = \begin{bmatrix} \mathbf{R}_M^A \; \mathbf{F}_{int} \\ \mathbf{R}_M^A \; \mathbf{M}_{int} + \mathbf{r}_{ee} \times \mathbf{R}_M^A \; \mathbf{F}_{int} \end{bmatrix} \quad (3)$$

where $\mathbf{F}_{int}$ and $\mathbf{M}_{int}$ represent the force and moment resulting from interaction, and $\mathbf{R}_M^A$ is the rotation matrix from frame $\mathcal{A}$ to frame $\mathcal{M}$.

In order to minimise forces and moments on the vehicle resulting from aerial interaction we need to address the terms $\mathbf{F}_{int}$, $\mathbf{M}_{int}$, and $\mathbf{r}_{ee}$. Hence, they become the three key design drivers as follows:

- design of an adaptively-compliant system that allows to absorb/filter the undesired forces $\mathbf{F}_{int}$ at the end-effector and mitigate the propagation of those to the aircraft.
- minimise the size of the end-effector in order to reduce the moment $\mathbf{M}_{int}$ transferred by the end-effector during interaction.
- design of a system which allows to move the location of the end-effector relative to the aircraft independently, so to reduce vector $\mathbf{r}_{ee}$.

III. Manipulator Design

In this section the mechanical design of the manipulation system and controller used are presented.

For the intended application of positioning of sensors, we propose a 2-DoF actuator that allows independent translation and pitching of the end-effector. The translational DoF is actuated by a brushless DC motor that drives a rack-and-pinion transmission, whilst the rotational DoF is provided by a servo motor which allows independent pitch of the end-effector. The design of the manipulator is illustrated in fig. 3. The end-effector is embodied by the tip of the rack that can house a sensor device, stored inside a case. For the purpose of the initial results, the design of a bespoke gripper will be addressed at a later stage.

The platform selected to perform airborne experiments is the quadcopter Lumenier QAV400.® The chosen rotors allow the QAV400 to carry a payload up to 550gr, however we limit the manipulator mass to be 100gr lighter to avoid motors saturation and increase flight time. The aircraft main features are displayed in table I. To reduce the mass distribution on the vehicle and therefore minimise the overall inertia, the manipulator's heavier components are placed nearer to the UAV CoG and the design is kept compact.

As previously discussed, the manipulator behaves as a variable-stiffness element. The equivalent concept in mechanics is resembled by an active spring-damper system that can be tuned to generate different rigidities. This is achieved by creating an adjustable torsional spring through a variable-gain PID controller.

Controller

The analogy between PID and spring-damper systems is used to achieve variable-compliance on the rack. The proportional gain K_p provides the rack with a spring-like behaviour, while K_d generates a damped motor's response.
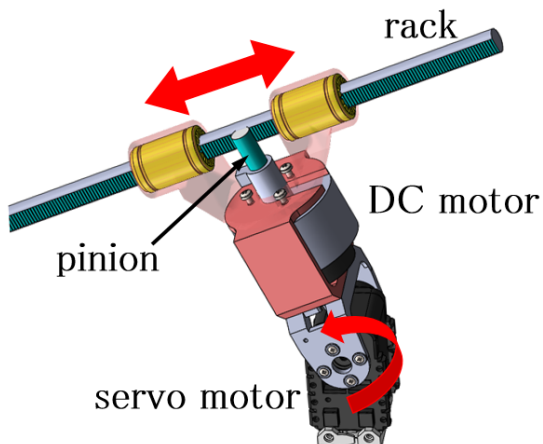

Fig. 3: Manipulator design: a servo motor provides pitching of the end-effector; translational motion results from a rack-and-pinion transmission driven by a DC motor. As the DC motor spins, the pinion drives a rack inside two linear bearings (in yellow). Motion of the rack is bidirectional.

TABLE I: Main features of the chosen aerial vehicle, quadcopter QAV400.

Total mass	Rotors	Battery	Flight time
1900gr	FX2216-9 1100kv	Lipo 3300mAh 4s	15+ minutes

TABLE II: Ziegler-Nichols parameters for PID controller.

K_u	T_u	K_p	K_i	K_d
8	0.045	4.8	214	0.027

The integral gain K_i is essential to overcome the system's stiction, i.e. below a certain threshold, the output sent by a PD type of controller cannot overcome the static friction of the motor and other mechanical parts.

The adjustable torsional spring effect is the outcome of a variable-gain PID controller: as an external force causes the rack to slide, translational motion is converted into rotational by the rack-and-pinion mechanism. At this stage the motor is forced to move away from a set reference position and an error generates. Thus, in order to minimise this error the motor will respond with a torque increase in the opposite direction. Both the torque and current outputted by the motor increase proportionally with the error.

By varying the PID gains, the manipulator can tailor to different needs. Lower gains generate a more compliant response to the forces exerted/absorbed by the end-effector; this is useful in a scenario where the vehicle approaches the wall at a high speed, or during a collision. On the other hand, higher gains will produce a more rigid behaviour and greater forces to achieve, for example, a placement tasks.

To tune the PID gains, the Ziegler-Nichols' rule is applied [24]. In table II the PID gains are listed, where K_u and T_u represent the ultimate gain and the oscillation period respectively for which stable and consistent oscillations occur.

IV. Simulation

The underlying assumptions discussed in section 2 and the design choices of section 3 are evaluated in Simulink® environment. In particular, we want to demonstrate the negative effect of a misplaced end-effector over the UAV attitude stability and the benefit of adaptive compliance over the forces experienced by the aircraft.

Model Description

It is assumed that the interaction takes place with a straight surface, e.g. a rigid wall, and no lateral forces, e.g. gusts, act on the aerial manipulator other than the interaction force. As the end-effector is designed to be small, contact is established at a single point, thus the resulting force lies on a plane.

In SimMechanics, we generate a planar model of aerial interaction where the UAV carries a 2-DoF manipulator. The rotational DoF is modeled by a revolute joint, and the translation one by a prismatic joint. Adaptive compliance is
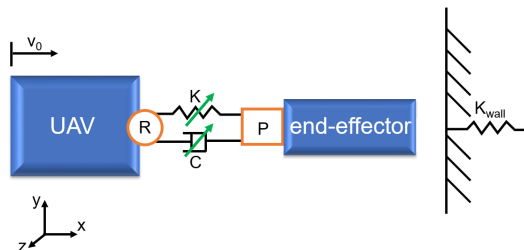

Fig. 4: Sketch of the planar model and relevant parameters.

modeled by means of a spring-damper mechanism where both the stiffness and damping coefficients are actively changed. The spring-damper mechanism guides the elastic behaviour of the prismatic joint. The UAV can perform planar motions, i.e. translation along *x-y* and rotation about the *z* axis. The initial condition on the UAV is a constant linear velocity $v_0 = 0.27$ m/sec directed towards the obstacle. A schematic diagram of the system can be seen in fig. 4.

The interaction between the two objects, i.e. the aerial manipulator and the obstacle, is recreated by means of a translational hard-stop constraint: the UAV is free to move along the *x* direction until the hard-stop bound is met and contact is established. This type of block is frequently used in SimMechanics to emulate collision of objects falling on the ground. Similarly the UAV is able to move forward with the given speed v_0 until the conditions of the hard-stop apply, then it is forced to stop. The obstacle object is modeled as a rectangular body with high stiffness and damping, e.g. a rigid wall. The geometry, inertias and mass properties of the actuator reflect those of commercial components. Likewise the aircraft model mimics the Lumenier QAV400® platform.

Simulation Results

In figure fig. 5 the angular displacement θ about the z axis, and the interaction torque $\mathbf{T}_{int}$ measured at the origin of frame $\mathcal{A}$ are illustrated. Both parameters display the effects of a different manipulator configuration on the aircraft CoG. The horizontal component $r_{ee,x}$ is chosen so

to protrude out of the aircraft's physical boundaries and to prevent interference with the rotors. The vertical component $r_{ee,y}$ is examined in three different scenarios: a positive $r_{ee,y}$ places the end-effector above the aircraft CoG, a negative $r_{ee,y}$ places it below its CoG and a null component makes the end-effector vertically aligned with the aircraft CoG.

As the tip of the end-effector moves along the vertical axis, the peak moment $\mathbf{T}_{int}$ is proportional to the magnitude of $r_{ee,y}$. Moreover, $\mathbf{T}_{int}$ has direction dependent on the sign of $r_{ee,y}$. A positive torque $\mathbf{T}_{int}$ generates clockwise when $r_{ee,y} > 0$, viceversa it is anti-clockwise with $r_{ee,y} < 0$, and null when the end-effector is vertically aligned with the aircraft CoG. This concept is illustrated in fig. 6.

The angular displacement θ increases exponentially after the collision takes place (at $t \approx 0.23$ sec), and reaches about $\pm 20°$ at t = 2.5 sec (outside figure boundaries). It is to be noted that the vehicle flight controller is not implemented in this model, hence the angle θ is not corrected by the UAV controller. In reality though, after an initial transition period the flight controller would act to stabilise the vehicle and counterbalance the induced moment.

In fig. 7 the interaction forces measured at the end-effector and at the UAV's CoG are illustrated. Both figures show the effects of varying the stiffness K [Nm] and damping coefficient C [N/(m/s)] of the linear actuator on the forces profile. Several conclusions can be drawn:

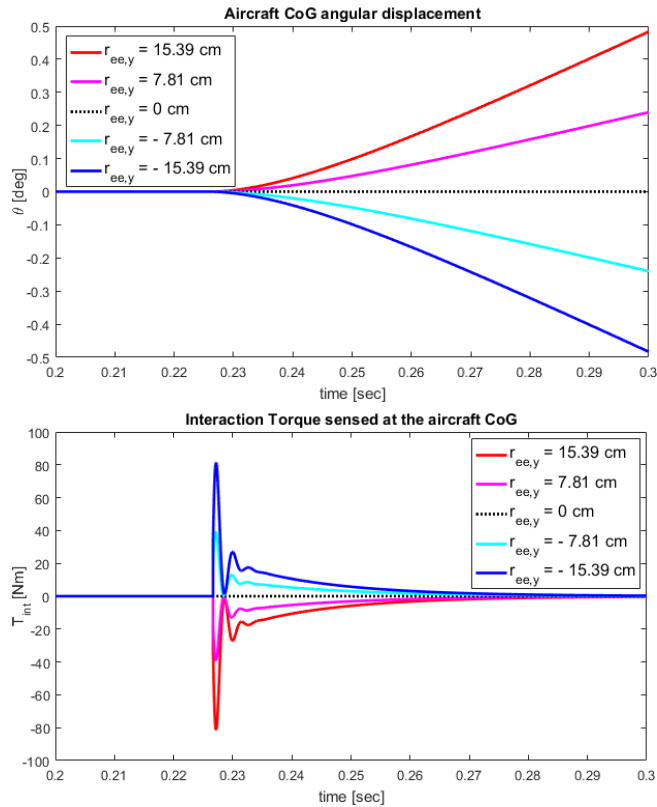- the presence of a spring-damper element on the manipu-

Fig. 5: The angular displacement and the torque sensed due to interaction are measured on the aircraft CoG using with different end-effector configurations. In particular we demonstrate the effect of the sign and magnitude of vector $r_{ee,y}$ over the torque $\mathbf{T}_{int}$.
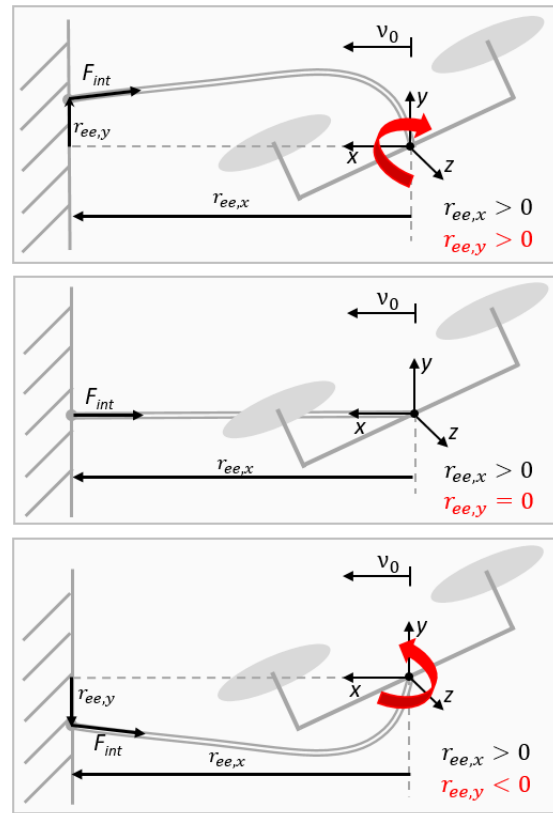

Fig. 6: Schematic representation of a UAV carrying a generic manipulator. The end-effector protrudes out in three different locations, changing the components of vector r_{ee}. The vertical component $r_{ee,y}$ affects the magnitude and direction of the moment resulting from $\mathbf{F}_{int}$.
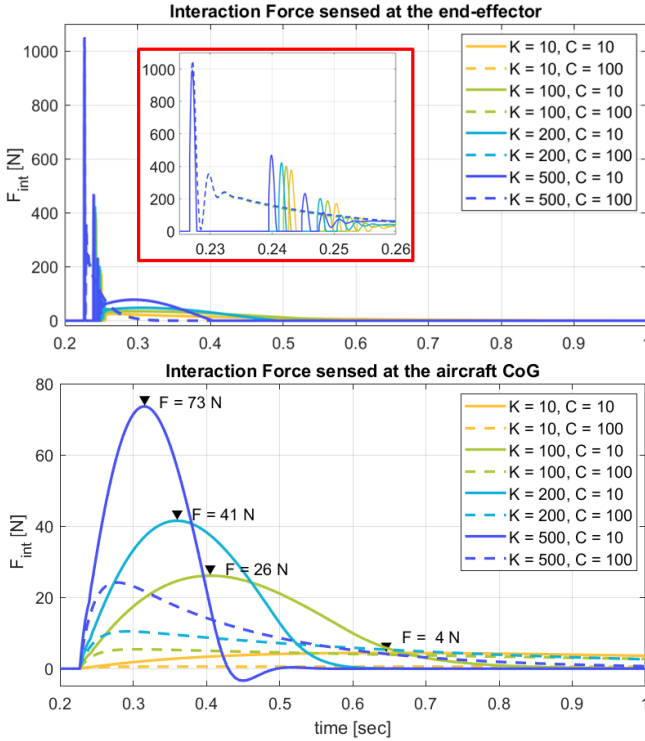
Fig. 7: A comparison of different stiffness K [Nm] and damping coefficients C [N/(m/s)] of the active spring-damper system. The interaction force is measured at two key locations: the end-effector (top figure) and the aircraft CoG (bottom figure). The response is substantially different due to the presence of compliance in the manipulator.

lator mitigates the forces experienced by the UAV CoG in magnitude, frequency and in the exponential decay;
- low stiffness values K produce forces that are lower in magnitude (yellow lines) and have a wider span over time, as opposed to high stiffness values (blue lines);
- higher values of damping coefficients C (dashed lines) are preferred over low values of C (solid lines) as damping dissipates the impact energy and causes the force to slowly decay over time.

Therefore, we can conclude that adaptive compliance brings a benefit to the aerial manipulator design as it allows to partially absorb the interaction forces, it prevents the vehicle from bouncing and it damps the propagated disturbances over time. Moreover, the location of the end-effector is a crucial design variable to minimise the induced interaction torques.

V. FLIGHT EXPERIMENTS

Several flight experiments are conducted to validate the behaviour of the proposed adaptive-compliance manipulator for aerial applications. To replicate the low-stiffness behaviours emerged from simulation, we sample three values for the proportional gain K_p at 10%, 20%, and 50% of the ultimate value K_u, respectively K_p = 0.8, 1.6, and 4. These are selected to be within the stable K_p value seen in table II. The derivative term K_d in table II appears very small in magnitude, hence we assume that changes in K_d would not affect compliance enough to perceive changes in forces.

Experimental Setup

The vehicle chosen for flight experiments is the QAV400. We select off-the-shelf components in Delrin material for the rack-and-pinion transmission, with a good trade-off between the mass and the rigidity of the material. A direct drive Maxon® motor EC 45 flat (50 Watt, 780 mNm stall torque, 150 gr, Hall sensor and encoder) actuates the motion of the rack. This motor is chosen for its ability to output high torques and therefore counteract high forces, such as those that could generate from an impact. A Dynamixel AX-12A servo motor drives the pitch of the end-effector and makes it vertically aligned with the vehicle CoG, so to replicate the configuration seen in fig. 6 (middle figure). A HC-SR04 ultrasound sensor is mounted at the front of the aircraft. The PID controller runs in an on-board computer with CAN bus capabilities. A 6-axis Force sensor (FTSens, IIT, Italy) is mounted on the wall where the interaction takes place. All flight experiments are conducted in a VICON motion capture system to acquire ground truth measurements of the UAV.

Flight Results

To recreate the initial conditions of the simulated model, the UAV is commanded to approach a wall with a constant speed of 0.25 m/sec and set PID gains at the actuator.

Figure 8 shows the force measured by the load cell during interaction. It is demonstrated that higher proportional gains K_p in the actuator controller instigate a stiffer behaviour at the end-effector and therefore generate higher contact forces. The peaks present in the same figure are due to the mechanical properties of the rack where the discrete structure of the teeth causes the force to spike while in contact.

The analogy between higher gains and higher forces was a repeatable outcome over 5 flight trials performed with the same K_p, as shown in table III, where the maximum force value for each flight and the average μ are listed.
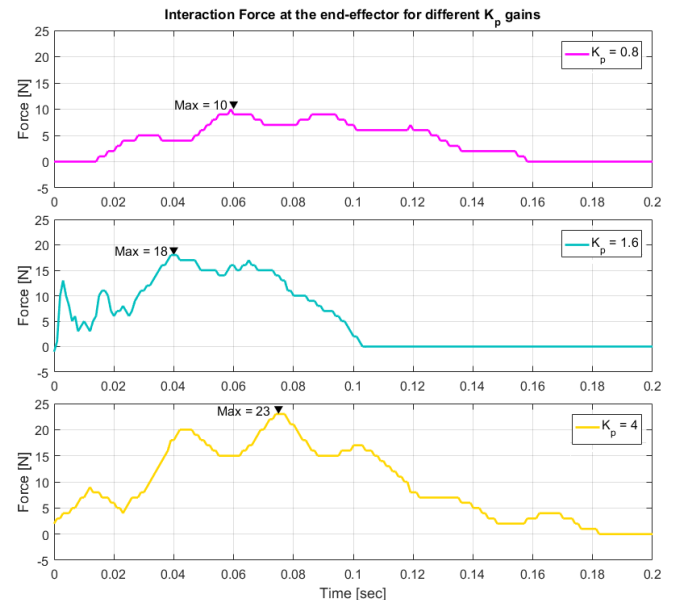

Fig. 8: A comparison of forces measured by the load cell during aerial interaction using a adaptive-compliance actuator.

TABLE III: Average μ and max values of forces measured during flight experiments with different compliance settings.

	trial #1	trial #2	trial #3	trial #4	trial #5	μ
$K_p = 0.8$	12	11	14	13	10	12
$K_p = 1.6$	14	13	14	18	16	15
$K_p = 4$	22	23	18	18	19	20

Comparing results obtained in simulation (fig. 7) with those obtained in real experiments (fig. 8) we notice how the forces behave alike: we obtain higher forces at the end-effector when pushing with a stiffer actuator. Instead, as we increase compliance, i.e. we reduce gain K_p, the magnitude of the force and the force response over time decrease. It is to be noted that the comparison between the simulated forces and the real ones is qualitative, as the simulated model does not include some important factors that play a role during airborne experiments, e.g. static friction of the components, energy dissipation, turbulence generated by the vehicle in the proximity of the wall.

VI. CONCLUSION

The state-of-the-art in aerial physical interaction has addressed operations carried out in quasi-static conditions. This work analyses the dynamics resulting from contact-based interaction and derives the key design parameters for a novel lightweight actuator intended for placement operations. In particular we propose a solution comprising a simple yet effective manipulator that features active variable-compliance and we demonstrate how such property is a necessity to provide different demanded forces at the end-effector. We tailor the design of the proposed actuator for the placement task of small objects, such as sensors, over vertical surfaces. We demonstrate how the end-effector location mitigates the resulting moments over the aircraft. Moreover, we carry out flight experiments where we equip a real vehicle with the proposed actuator and we validate its compliant behaviour over 15 flights. Successful airborne results demonstrate that the proposed actuator can tailor different forces at the end-effector by tuning its controller gains.

Future work will include incorporating force control for generating a precisely defined force curve over time. Moreover, other methods to achieve active compliance through the use of soft materials will be explored.

REFERENCES

[1] M. Bernard and K. Kondak, "Generic slung load transportation system using small size helicopters," in *Robotics and Automation, 2009. ICRA'09. IEEE International Conference on*, pp. 3258–3264, IEEE, 2009.

[2] S. Kim, S. Choi, and H. J. Kim, "Aerial manipulation using a quadrotor with a two dof robotic arm," in *Intelligent Robots and Systems (IROS), 2013 IEEE/RSJ International Conference on*, pp. 4990–4995, IEEE, 2013.

[3] S. B. Backus, L. U. Odhner, and A. M. Dollar, "Design of hands for aerial manipulation: Actuator number and routing for grasping and perching," in *Intelligent Robots and Systems (IROS 2014), 2014 IEEE/RSJ International Conference on*, pp. 34–40, IEEE, 2014.

[4] K. Kondak, A. Ollero, I. Maza, K. Krieger, A. Albu-Schaeffer, M. Schwarzbach, and M. Laiacker, "Unmanned aerial systems physically interacting with the environment: Load transportation, deployment, and aerial manipulation," in *Handbook of Unmanned Aerial Vehicles*, pp. 2755–2785, Springer, 2015.

[5] N. Michael, J. Fink, and V. Kumar, "Cooperative manipulation and transportation with aerial robots," *Autonomous Robots*, vol. 30, no. 1, pp. 73–86, 2011.

[6] D. Mellinger, Q. Lindsey, M. Shomin, and V. Kumar, "Design, modeling, estimation and control for aerial grasping and manipulation," in *Intelligent Robots and Systems (IROS), 2011 IEEE/RSJ International Conference on*, pp. 2668–2673, IEEE, 2011.

[7] P. E. Pounds, D. R. Bersak, and A. M. Dollar, "Grasping from the air: Hovering capture and load stability," in *Robotics and Automation (ICRA), 2011 IEEE International Conference on*, pp. 2491–2498, IEEE, 2011.

[8] M. Fumagalli, R. Naldi, A. Macchelli, F. Forte, A. Q. Keemink, S. Stramigioli, R. Carloni, and L. Marconi, "Developing an aerial manipulator prototype: Physical interaction with the environment," *Robotics & Automation Magazine, IEEE*, vol. 21, no. 3, pp. 41–50, 2014.

[9] A. Albers, S. Trautmann, T. Howard, T. A. Nguyen, M. Frietsch, and C. Sauter, "Semi-autonomous flying robot for physical interaction with environment," in *Robotics Automation and Mechatronics (RAM), 2010 IEEE Conference on*, pp. 441–446, IEEE, 2010.

[10] M. Orsag, C. Korpela, and P. Oh, "Modeling and control of mm-uav: Mobile manipulating unmanned aerial vehicle," *Journal of Intelligent & Robotic Systems*, vol. 69, no. 1-4, pp. 227–240, 2013.

[11] M. Orsag, C. Korpela, S. Bogdan, and P. Oh, "Valve turning using a dual-arm aerial manipulator," in *Unmanned Aircraft Systems (ICUAS), 2014 International Conference on*, pp. 836–841, IEEE, 2014.

[12] J. L. Scholten, M. Fumagalli, S. Stramigioli, and R. Carloni, "Interaction control of an uav endowed with a manipulator," in *Robotics and Automation (ICRA), 2013 IEEE International Conference on*, pp. 4910–4915, IEEE, 2013.

[13] T. Bartelds, A. Capra, S. Hamaza, S. Stramigioli, and M. Fumagalli, "Compliant aerial manipulators: Towards a new generation of aerial robotic workers,"

[14] J. T. Bartelds, "Understanding the critical design parameters of aerial manipulators during physical interaction," msc report 022ram2015, University of Twente, Aug. 2015.

[15] A. Suarez, G. Heredia, and A. Ollero, "Lightweight compliant arm for aerial manipulation," in *Intelligent Robots and Systems (IROS), 2015 IEEE/RSJ International Conference on*, pp. 1627–1632, IEEE, 2015.

[16] A. Suarez, G. Heredia, and A. Ollero, "Lightweight compliant arm with compliant finger for aerial manipulation and inspection," in *Intelligent Robots and Systems (IROS), 2016 IEEE/RSJ International Conference on*, pp. 4449–4454, IEEE, 2016.

[17] C. J. Salaan, K. Tadakuma, Y. Okada, E. Takane, K. Ohno, and S. Tadokoro, "Uav with two passive rotating hemispherical shells for physical interaction and power tethering in a complex environment," in *Robotics and Automation (ICRA), 2017 IEEE International Conference on*, pp. 3305–3312, IEEE, 2017.

[18] A. Briod, P. Kornatowski, J.-C. Zufferey, and D. Floreano, "A collision-resilient flying robot," *Journal of Field Robotics*, vol. 31, no. 4, pp. 496–509, 2014.

[19] M. Bisgaard, A. la Cour-Harbo, and J. D. Bendtsen, "Adaptive control system for autonomous helicopter slung load operations," *Control Engineering Practice*, vol. 18, no. 7, pp. 800–811, 2010.

[20] F. Forte, R. Naldi, A. Macchelli, and L. Marconi, "Impedance control of an aerial manipulator," in *American Control Conference (ACC), 2012*, pp. 3839–3844, IEEE, 2012.

[21] G. Giglio and F. Pierri, "Selective compliance control for an unmanned aerial vehicle with a robotic arm," in *Control and Automation (MED), 2014 22nd Mediterranean Conference of*, pp. 1190–1195, IEEE, 2014.

[22] C. Korpela, M. Orsag, T. Danko, B. Kobe, C. McNeil, R. Pisch, and P. Oh, "Flight stability in aerial redundant manipulators," in *Robotics and Automation (ICRA), 2012 IEEE International Conference on*, pp. 3529–3530, IEEE, 2012.

[23] I. Palunko, P. Cruz, and R. Fierro, "Agile load transportation: Safe and efficient load manipulation with aerial robots," *IEEE Robotics & Automation Magazine*, vol. 19, no. 3, pp. 69–79, 2012.

[24] J. G. Ziegler and N. B. Nichols, "Optimum settings for automatic controllers," *trans. ASME*, vol. 64, no. 11, 1942.